

neurons by producing large random fluctuations in the membrane potential<sup>7</sup>. In such models, however, it is only the average rate of excitatory and inhibitory postsynaptic potentials that is balanced; the individual events occur at random times, like raindrops. By contrast, the tight coordination we observed reflects a more precise control of cortical circuitry, unlikely to arise from random and independent synaptic activity arriving at a uniform rate<sup>30</sup>. Moreover, the rapid quenching of excitation by inhibition limits the window available for temporal summation, enabling neurons to behave as coincidence detectors and thereby increasing temporal precision<sup>6</sup>.

We illustrate this distinction by using a simple integrate-and-fire model (Fig. 5). Balanced but delayed inhibition decreased the trial-to-trial jitter in output spike times compared with the jitter in the input spike times (from 1 ms to 0.6 ms; Fig. 5a), whereas excitation and inhibition that were balanced on average instead increased spike time jitter (from 1 ms to 4.7 ms; Fig. 5b). In both of these models, excitation and inhibition are balanced, but in a different sense: a continuing balance produces irregular firing (similar to responses observed in visual cortex, which motivate such models), whereas the transient and temporally offset balance we have observed produces highly transient spiking responses (Figs 1d and 3c), which is consistent with previous findings in auditory cortex<sup>3,27,28</sup>. Thus our data suggest that balanced inhibition can sharpen neural responses in time, reducing rather than increasing the randomness of cortical operation. □

## Methods

We recorded from 62 cells in primary auditory cortex (all subpial depths) of anaesthetized (ketamine-medetomidine) rats aged 17–24 days after birth, using standard blind *in vivo* whole-cell methods. Pure tones had a duration of either 25 ms with a 5 ms 10–90% cosine-squared ramp, or 70 ms with a 20 ms ramp, and were delivered free-field at a rate of 1–2 per second using a calibrated electrostatic speaker in a double-walled sound booth. Total synaptic conductance, corrected for series resistance, was computed assuming an isopotential neuron (see Supplementary Methods for further details).

Received 17 March; accepted 10 October 2003; doi:10.1038/nature02116.

- Shamma, S. A. & Symmes, D. Patterns of inhibition in auditory cortical cells in awake squirrel monkeys. *Hear. Res.* **19**, 1–13 (1985).
- Calford, M. B. & Semple, M. N. Monaural inhibition in cat auditory cortex. *J. Neurophysiol.* **73**, 1876–1891 (1995).
- Sutter, M. L., Schreiner, C. E., McLean, M., O'Connor, K. N. & Loftus, W. C. Organization of inhibitory frequency receptive fields in cat primary auditory cortex. *J. Neurophysiol.* **82**, 2358–2371 (1999).
- Chen, Q. C. & Jen, P. H. Bicuculline application affects discharge patterns, rate-intensity functions, and frequency tuning characteristics of bat auditory cortical neurons. *Hear. Res.* **150**, 161–174 (2000).
- Wang, J., McFadden, S. L., Caspary, D. & Salvi, R. Gamma-aminobutyric acid circuits shape response properties of auditory cortex neurons. *Brain Res.* **944**, 219–231 (2002).
- Pouille, F. & Scanziani, M. Enforcement of temporal fidelity in pyramidal cells by somatic feed-forward inhibition. *Science* **293**, 1159–1163 (2001).
- Shadlen, M. N. & Newsome, W. T. The variable discharge of cortical neurons: implications for connectivity, computation, and information coding. *J. Neurosci.* **18**, 3870–3896 (1998).
- Hartline, H. K., Wagner, H. G. & Ratcliff, F. Inhibition in the eye of *Limulus*. *J. Gen. Physiol.* **39**, 651–673 (1956).
- Zhang, L. I., Tan, A. Y., Schreiner, C. E. & Merzenich, M. M. Topography and synaptic shaping of direction selectivity in primary auditory cortex. *Nature* **424**, 201–205 (2003).
- Borg-Graham, L. J., Monier, C. & Fregnac, Y. Visual input evokes transient and strong shunting inhibition in visual cortical neurons. *Nature* **393**, 369–373 (1998).
- Hirsch, J. A., Alonso, J. M., Reid, R. C. & Martinez, L. M. Synaptic integration in striate cortical simple cells. *J. Neurosci.* **18**, 9517–9528 (1998).
- Anderson, J. S., Carandini, M. & Ferster, D. Orientation tuning of input conductance, excitation, and inhibition in cat primary visual cortex. *J. Neurophysiol.* **84**, 909–926 (2000).
- Monier, C., Chavane, F., Baudot, P., Graham, L. J. & Fregnac, Y. Orientation and direction selectivity of synaptic inputs in visual cortical neurons: a diversity of combinations produces spike tuning. *Neuron* **37**, 663–680 (2003).
- Moore, C. I. & Nelson, S. B. Spatio-temporal subthreshold receptive fields in the vibrissa representation of rat primary somatosensory cortex. *J. Neurophysiol.* **80**, 2882–2892 (1998).
- Carandini, M. & Ferster, D. Membrane potential and firing rate in cat primary visual cortex. *J. Neurosci.* **20**, 470–484 (2000).
- Ojima, H. & Murakami, K. Intracellular characterization of suppressive responses in supragranular pyramidal neurons of cat primary auditory cortex *in vivo*. *Cereb. Cortex* **12**, 1079–1091 (2002).
- Chung, S. & Ferster, D. Strength and orientation tuning of the thalamic input to simple cells revealed by electrically evoked cortical suppression. *Neuron* **20**, 1177–1189 (1998).
- Miller, L. M., Escabi, M. A., Read, H. L. & Schreiner, C. E. Functional convergence of response properties in the auditory thalamocortical system. *Neuron* **32**, 151–160 (2001).
- Schummers, J., Marino, J. & Sur, M. Synaptic integration by V1 neurons depends on location within the orientation map. *Neuron* **36**, 969–978 (2002).

- Phillips, D. P. & Cynader, M. S. Some neural mechanisms in the cat's auditory cortex underlying sensitivity to combined tone and wide-spectrum noise stimuli. *Hear. Res.* **18**, 87–102 (1985).
- Volkov, I. O. & Galazyuk, A. V. Peculiarities of inhibition in cat auditory cortex neurons evoked by tonal stimuli of various durations. *Exp. Brain Res.* **91**, 115–120 (1992).
- Chung, S., Li, X. & Nelson, S. Short-term depression at thalamocortical synapses contributes to rapid adaptation of cortical sensory responses *in vivo*. *Neuron* **34**, 437–446 (2002).
- Chance, F. S., Abbott, L. F. & Reyes, A. D. Gain modulation from background synaptic input. *Neuron* **35**, 773–782 (2002).
- Phillips, D. P. Effect of tone-pulse rise time on rate-level functions of cat auditory cortex neurons: excitatory and inhibitory processes shaping responses to tone onset. *J. Neurophysiol.* **59**, 1524–1539 (1988).
- De Ribaupierre, F., Goldstein, M. H. Jr & Yeni-Komshian, G. Intracellular study of the cat's primary auditory cortex. *Brain Res.* **48**, 185–204 (1972).
- Mitani, A. & Shimokouchi, M. Neuronal connections in the primary auditory cortex: an electrophysiological study in the cat. *J. Comp. Neurol.* **235**, 417–429 (1985).
- Brugge, J. E., Dubrovsky, N. A., Aitkin, L. M. & Anderson, D. J. Sensitivity of single neurons in auditory cortex of cat to binaural tonal stimulation; effects of varying interaural time and intensity. *J. Neurophysiol.* **32**, 1005–1024 (1969).
- DeWeese, M. R., Wehr, M. & Zador, A. M. Binary spiking in auditory cortex. *J. Neurosci.* **23**, 7940–7949 (2003).
- Covey, E., Kauer, J. A. & Casseday, J. H. Whole-cell patch-clamp recording reveals subthreshold sound-evoked postsynaptic currents in the inferior colliculus of awake bats. *J. Neurosci.* **16**, 3009–3018 (1996).
- Stevens, C. F. & Zador, A. M. Input synchrony and the irregular firing of cortical neurons. *Nature Neurosci.* **1**, 210–217 (1998).

Supplementary Information accompanies this paper on [www.nature.com/nature](http://www.nature.com/nature).

**Acknowledgements** We thank K. Miller, L. Miller, M. Kvale, Z. Mainen, M. DeWeese and M. Sutter for comments on an earlier version of this manuscript. This work has been supported by grants to A.M.Z. from the Packard Foundation, the Sloan Foundation, the NIH and the Mathers Foundation.

**Competing interests statement** The authors declare that they have no competing financial interests.

**Correspondence** and requests for materials should be addressed to A.M.Z. ([zador@cshl.edu](mailto:zador@cshl.edu))

## An ancient role for nuclear $\beta$ -catenin in the evolution of axial polarity and germ layer segregation

Athula H. Wikramanayake<sup>1</sup>, Melanie Hong<sup>1,2</sup>, Patricia N. Lee<sup>2</sup>, Kevin Pang<sup>2</sup>, Christine A. Byrum<sup>1</sup>, Joanna M. Bince<sup>1</sup>, Ronghui Xu<sup>1</sup> & Mark Q. Martindale<sup>2</sup>

<sup>1</sup>Department of Zoology, University of Hawaii at Manoa, 2538 McCarthy Mall, Honolulu 96822, Hawaii

<sup>2</sup>Kewalo Marine Lab/Pacific Biomedical Research Center, University of Hawaii, 41 Ahui Street, Honolulu 96813, Hawaii

The human oncogene  $\beta$ -catenin is a bifunctional protein with critical roles in both cell adhesion and transcriptional regulation in the Wnt pathway<sup>1–3</sup>. Wnt/ $\beta$ -catenin signalling has been implicated in developmental processes as diverse as elaboration of embryonic polarity<sup>2–6</sup>, formation of germ layers<sup>4–8</sup>, neural patterning, spindle orientation and gap junction communication<sup>2</sup>, but the ancestral function of  $\beta$ -catenin remains unclear. In many animal embryos, activation of  $\beta$ -catenin signalling occurs in blastomeres that mark the site of gastrulation and endomesoderm formation<sup>5–10</sup>, raising the possibility that asymmetric activation of  $\beta$ -catenin signalling specified embryonic polarity and segregated germ layers in the common ancestor of bilaterally symmetrical animals. To test whether nuclear translocation of  $\beta$ -catenin is involved in axial identity and/or germ layer formation in 'pre-bilaterians', we examined the *in vivo* distribution, stability and function of  $\beta$ -catenin protein in embryos of the sea anemone *Nematostella vectensis* (Cnidaria, Anthozoa). Here we

show that *N. vectensis*  $\beta$ -catenin is differentially stabilized along the oral–aboral axis, translocated into nuclei in cells at the site of gastrulation and used to specify entoderm, indicating an evolutionarily ancient role for this protein in early pattern formation.

Anthozoans (sea anemones and corals) are basal members of the Cnidaria, a diverse and highly successful phylum, which is the sister group to bilaterian metazoans<sup>11,12</sup>. Unlike triploblastic bilaterians, which possess derivatives of three embryonic germ layers and are bilaterally symmetrical, cnidarians possess only two germ layers (an external ectodermal layer and internal entodermal layer) and are said to be radially symmetrical around the major longitudinal oral–aboral axis. The evolutionary relationships of the anterior–posterior and dorsoventral axes between bilaterally and radially symmetrical animals remain enigmatic, but as an outgroup to bilaterians, diploblastic cnidarians provide insight into bilaterian development and evolution.

*N. vectensis* is a small, solitary dioecious sea anemone with a simple life cycle<sup>13</sup>. As with other cnidarian oocytes<sup>14</sup>, unfertilized *N. vectensis* oocytes do not appear to have a fixed polarity (that is, animal–vegetal axis). Rather, the adult oral–aboral axis is determined at the time of first cleavage. Gastrulation produces a ciliated, bilayered planula that transforms into an epithelial polyp with an outer ectodermal layer and an inner bifunctional (with both absorptive and contractile properties) entodermal gastrodermis lining the gastric cavity. The molecular mechanisms directing the polarization of an apparently symmetrical cnidarian egg and the segregation of the two germ layers are poorly understood<sup>14</sup>, but are critical for understanding the evolution of triploblastic, bilaterally symmetrical animals from a presumed diploblastic, radially symmetrical ancestor<sup>15</sup>.

Previous studies indicate a role for the Wnt signalling pathway in axis formation during adult asexual budding in *Hydra*, a derived freshwater hydrozoan<sup>16</sup>. However, these studies did not address the role of Wnt signalling during embryogenesis. To determine whether the Wnt signalling pathway functions during early embryogenesis

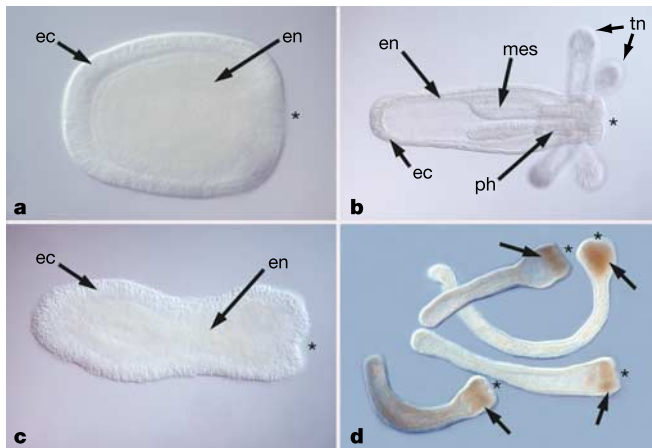


**Figure 1** Lithium chloride treatment of *N. vectensis* embryos results in the hyperproliferation of entoderm at gastrulation. **a**, A normal 3-day-old planula stage embryo consisting of an outer ectoderm (ec) and a solid ball of entodermal (en) precursors that have entered through the position of the blastopore (asterisks in all panels). **b**, A 7-day-old juvenile polyp with definitive ectodermal and entodermal germ layers. Entoderm lines the gastric cavity and feeding tentacles (tn) are associated with the site of gastrulation (mouth/anus). The lining of the pharynx (ph) and directive mesenteries (mes) are ectodermal in origin. **c**, A 3-day-old planula treated with 20 mM LiCl from early cleavage stages. The planula elongates as cells continue to enter the blastocoel during gastrulation. **d**, A 7-day-old lithium-treated planula. Both ectodermal and entodermal germ layers have formed, but the ectodermal components of the tentacles and pharynx have failed to form at the expense of entodermal proliferation (arrows).

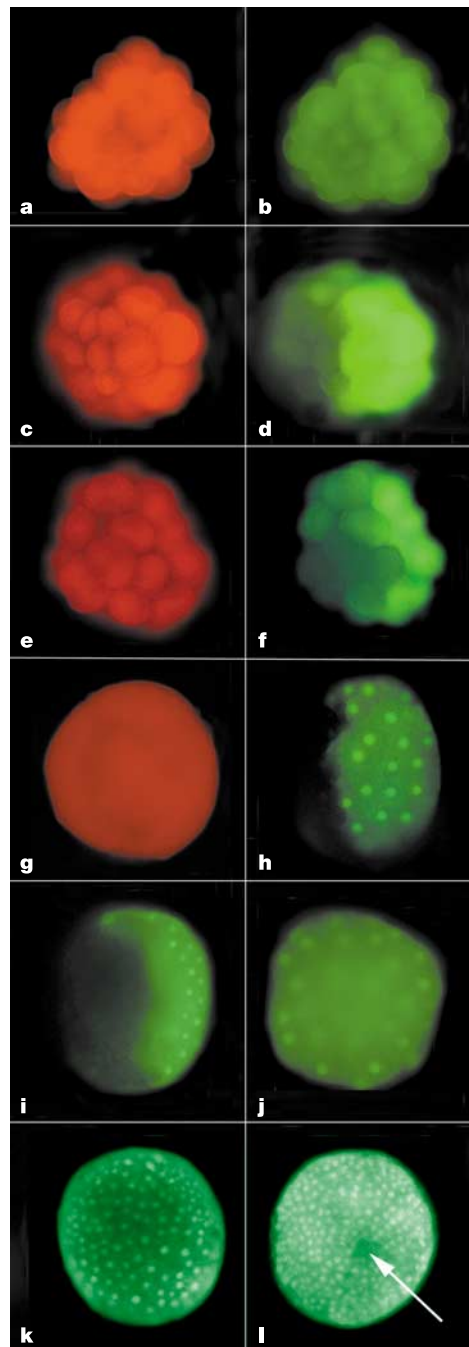


**Figure 2** The temporal and spatial dynamics of  $\beta$ -catenin–GFP protein in live *N. vectensis* embryos. mRNA coding for the fusion protein (green) was co-injected with rhodamine dextran (red) into zygotes. All images are oriented with the future oral pole to the right. **a, c, e** and **g** are fluorescent images of the injected embryos seen in **b, d, f** and **h** showing uniform distribution of rhodamine dextran throughout the embryo. **b**, Nv $\beta$ -cat–GFP protein expression is detected within an hour of injection and is uniformly expressed in the early embryo. At approximately the 32-cell stage, Nv $\beta$ -cat–GFP protein is degraded at one pole of the embryo, but remains highly expressed at the other pole (**d, f**). GFP fluorescence remains intense at the blastula stage at the pole where gastrulation will occur, and the protein enters the nuclei of entodermal precursors (**h**). **i**, A late blastula stage *N. vectensis* embryo developing from a zygote injected with *Xenopus*  $\beta$ -catenin–GFP chimaeric mRNA. Selective stabilization and nuclear localization of this chimaeric protein is identical to the behaviour of Nv $\beta$ -cat–GFP. **j**, Injection of a stabilized *Xenopus*  $\beta$ -catenin–GFP mRNA into *N. vectensis* zygotes results in uniform expression and nuclear entry of the protein into all blastomeres of the developing embryos. **k, l**, 20 mM lithium chloride treatment of Nv $\beta$ -cat–GFP mRNA injected zygotes results in the expanded domains of  $\beta$ -catenin–GFP nuclearization, as expected by GSK-3 $\beta$  inactivation, at six (**k**) and eight (**l**) hours post injection. The arrow indicates the blastopore in **l**.

in cnidarians, we treated *N. vectensis* zygotes with lithium chloride (LiCl), which interferes with glycogen synthase kinase-3 $\beta$  (GSK-3 $\beta$ )-mediated degradation of  $\beta$ -catenin in the Wnt signalling cascade<sup>17</sup>. Exposing *N. vectensis* embryos to 10–40 mM LiCl resulted in elongated planulae that fail to make an ectodermal pharynx or tentacles (Fig. 1c, d). Defects in these embryos were first observed during gastrulation with a dramatic increase in endodermal precursors, a classic phenomenon known as “vegetalization”<sup>18</sup>.

The effects of lithium on gastrulation movements and germ layer formation led us to follow the spatial and temporal dynamics of  $\beta$ -catenin in live *N. vectensis* embryos using a *N. vectensis*  $\beta$ -catenin (Nv $\beta$ -catenin):green fluorescent protein fusion protein (Nv $\beta$ -cat-GFP). Structure-function analysis of the Nv $\beta$ -catenin molecule has shown that, although many amino- and carboxy-terminal protein-protein interaction domains found in bilaterian  $\beta$ -catenins appear to be absent, both cell adhesion and cell signalling domains are present<sup>19</sup>. Microinjection of *in vitro* synthesized Nv $\beta$ -cat-GFP messenger RNA into fertilized *N. vectensis* eggs results in uniform cytoplasmic expression of this fusion protein throughout the entire embryo during the initial cleavage stages (Fig. 2a, b). However, between the 16-cell and 60-cell stages degradation of Nv $\beta$ -cat-GFP begins in approximately one-half of the embryo (Fig. 2c–f) as detected by the loss of GFP fluorescence. By the 60-cell stage GFP fluorescence is completely lost in approximately one-half of the embryo, while cells in the other half retain high levels of the fusion protein in the cytoplasm, where it clearly enters the nuclei (Fig. 2g, h). Following GFP expression to later stages showed that Nv $\beta$ -cat-GFP persists in cells at the future oral pole and remains in cells that enter the blastocoel during gastrulation. Identical results were obtained when chimaeric *Xenopus*  $\beta$ -catenin-GFP mRNA<sup>20</sup> was injected into *N. vectensis* embryos (Fig. 2i). Almost identical results have been reported in sea urchin embryos<sup>21</sup>, indicating that a

similar mechanism of protein regulation may have existed in the common ancestor to all eumetazoans.

To verify that the endogenous Nv $\beta$ -cat protein displays temporal and spatial dynamics similar to those of Nv $\beta$ -cat-GFP, we used a cross-reactive affinity-purified anti-*Xenopus*  $\beta$ -catenin antibody to localize the protein in early *N. vectensis* embryos (see Supplementary Information). Endogenous  $\beta$ -catenin protein was detected in a subset of nuclei beginning at the 16–32-cell stages (Fig. 3a). By the early and mid-blastula stage, approximately half the blastomeres in the embryos have strong nuclear staining, whereas the remaining blastomeres have little or no nuclear staining (Fig. 3b). The blastomeres with nuclear-localized Nv $\beta$ -cat at the blastula stage appear to be cells that form endoderm as immunolocalization of Nv $\beta$ -catenin at the initial stages of gastrulation shows intense staining in invaginating cells (Fig. 3c) as predicted from the dynamics of Nv $\beta$ -cat-GFP (Fig. 2). Nuclear  $\beta$ -catenin thus provides the first known molecular index of axial asymmetry in *N. vectensis* embryos and this nuclearization is correlated with the site of endoderm formation and gastrulation.

One mechanism of regulating the concentration of  $\beta$ -catenin in cells is the targeting of this protein for degradation by a GSK-3 $\beta$ - and casein kinase-1-dependent phosphorylation of a cluster of four residues on the amino terminus<sup>22,23</sup>. Structural analyses have shown that this phosphorylation motif is conserved in  $\beta$ -catenin from humans to cnidarians<sup>19,23</sup>. To determine whether this aspect of Wnt signalling is conserved in *N. vectensis* we examined the expression and localization of an ‘activated’ form of *Xenopus*  $\beta$ -catenin fused to GFP, in which the GSK-3 $\beta$ /CK-1 phosphorylation sites had been

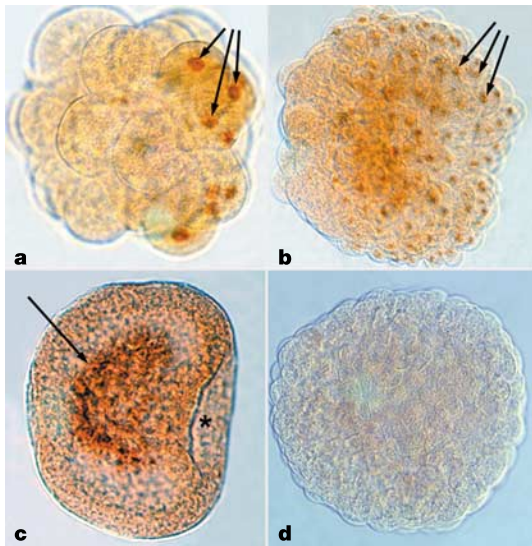


**Figure 3** Immunohistochemical localization of endogenous *N. vectensis*  $\beta$ -catenin. **a**, A 32-cell stage *N. vectensis* embryo labelled with an anti- $\beta$ -catenin antibody. Intense nuclear staining is seen in cells on one side of the embryo but not in the other. **b**, Oblique view of a blastula stage *N. vectensis* embryo labelled with the anti- $\beta$ -catenin antibody. Nuclear staining is seen on only one side of the embryo corroborating the spatial dynamics of the Nv $\beta$ -cat-GFP chimaeric protein. **c**, Early gastrula stage embryo labelled with the anti- $\beta$ -catenin antibody. Intense staining is seen in the developing endoderm. The asterisk marks the blastopore. **d**, A blastula stage embryo that was incubated with the anti- $\beta$ -catenin antibody following pre-adsorption with a purified bacterially produced Nv $\beta$ -catenin fusion protein. No staining is seen in the embryos. Arrows point to nuclear  $\beta$ -catenin in **a** and **b** and cytoplasmic  $\beta$ -catenin in the endoderm in **c**.

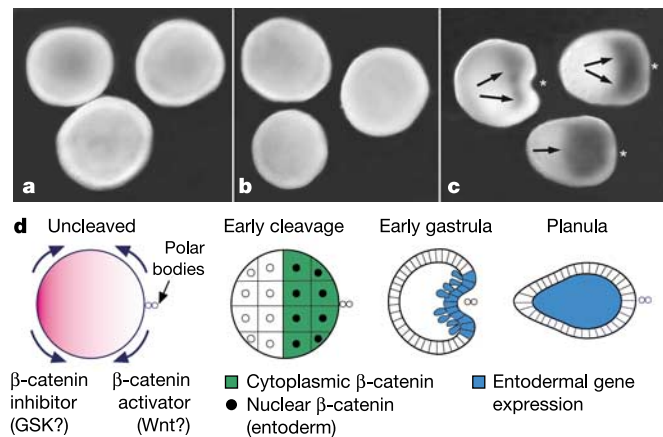


**Figure 4** Blocking the nuclear function of  $\beta$ -catenin inhibits endoderm formation in *N. vectensis*. **a**, Injection of *in vitro* synthesized mRNA for sea urchin cadherin—a molecule that binds  $\beta$ -catenin and reduces its free concentration—prevents gastrulation. Injected embryos fail to gastrulate and remain a hollow ball of cells even after 30 h. **b**, Fusion of the transcriptional repression domain from the *Drosophila engrailed* gene to  $\beta$ -catenin generates a chimaeric protein that binds DNA but does not activate downstream targets. The injection of *in vitro* synthesized mRNA coding for this fusion protein also results in the complete absence of gastrulation and endoderm formation. **c**, Control embryos showing endodermal cells (arrows) that have entered the blastocoel through the blastopore (asterisks). The top left embryo is 10 h, the top right embryo 24 h, and the bottom embryo is 30 h post first cleavage. **d**, Model indicating the possible origin of germ layers in a diploblastic embryo. An initial signal generated by the sperm and/or first cleavage polarizes the embryo. This initial polarization event reorganizes the  $\beta$ -catenin destruction machinery, so that it either removes an inhibitor of canonical Wnt signalling from the future oral pole (GSK?) or it localizes an activator of the pathway (Wnt?) to the future oral pole. The stabilization of  $\beta$ -catenin in one hemisphere allows the nuclearization of the protein in cells at the site of gastrulation where it acts as a transcriptional co-activator of specific genes necessary for endoderm specification and gastrulation. The polar bodies mark the future oral pole.

mutated to alanines<sup>22</sup>. Embryos developing from fertilized eggs injected with an mRNA coding for this chimaeric protein showed GFP-mediated fluorescence in all cells of the blastula, well after it begins to be degraded in normal embryos, and nuclear translocation of Nvβ-cat-GFP in all blastomeres (Fig. 2j). Lithium chloride treatment of Nvβ-cat-GFP injected zygotes also has the expected result of an expansion of the domain of β-catenin nuclear localization (Fig. 2k, l). These results indicate that much of the complex post-translational regulation of β-catenin destabilization has been conserved in the Metazoa.

In many animal embryos, blocking β-catenin signalling results in failure of germ layer segregation and/or disruption of gastrulation<sup>2–8,24</sup>. To determine whether β-catenin signalling plays a functional role in early segregation of germ layers in a diploblastic animal, we carried out a loss-of-function experiment designed to competitively titrate β-catenin from the nucleus by overexpressing cadherin<sup>4–6,24</sup>. Embryos developing from cadherin mRNA-injected zygotes (Fig. 4a) fail to invaginate or gastrulate even after control animals have completed gastrulation (Fig. 4c). To verify that the phenotype was specific to loss of β-catenin signalling, and not a cell adhesion defect caused by cadherin overexpression, we blocked β-catenin-dependent transcription by overexpressing a β-catenin-engrailed repressor-domain fusion protein that has been shown to block β-catenin-dependent transcription<sup>25</sup>. Injection of β-catenin-engrailed mRNA results in embryos that have phenotypes identical to the cadherin-overexpressing embryos, indicating that the phenotype is generated specifically by loss of β-catenin signalling in *N. vectensis* embryos (Fig. 4b). These data provide compelling evidence that the downstream components of the canonical Wnt signalling pathway are asymmetrically activated during early embryogenesis and are used for the initial segregation of germ layers in a basal cnidarian embryo. We do not know at present whether this asymmetry in nuclear localization of Nvβ-catenin is driven by Wnt signals or perhaps by asymmetries created by the fertilizing sperm. It is of some interest that in hydrozoan embryos, sperm can only enter the egg at the site of polar-body formation<sup>26</sup>, which is the same pole that accumulates nuclear β-catenin in *N. vectensis* and gives rise to endoderm.

Our results indicate a key role for the Wnt/β-catenin pathway in the evolution of axial asymmetries and endoderm formation in an ancestor that existed before the evolution of the mesodermal germ layer. The lack of a fixed maternal animal–vegetal axis that can serve as a scaffold for axial patterning in cnidarians<sup>14</sup> suggests that the initial molecular asymmetry in these embryos is achieved by a post-fertilization reorganization of the egg cytoplasm that leads to the selective degradation of β-catenin at one pole, and stabilization and subsequent nuclear accumulation in the endoderm-forming pole (Fig. 4d). The observation that similar selective accumulation of β-catenin at one embryonic pole also occurs in deuterostome embryos<sup>21,27</sup> indicates that this mechanism evolved early during animal evolution and was recruited for generating axial polarities during embryogenesis. We speculate that the evolution of a mechanism to nuclearize β-catenin asymmetrically during early development was the innovation that led to the initial segregation of germ layers from a single-layered blastula-like organism during animal evolution. □

**Methods**

**DNA constructs**

A *N. vectensis* PCR fragment corresponding to amino acids 302–656 of mouse β-catenin<sup>19</sup> was digested with *Hind*III and *Not*I to release an 876 base pair (bp) fragment. *N. vectensis* gene-specific primer 1 (5'-TGGGCAGCTTCTGCATCGGCGTGACGGC-3') was used to carry out 5' RACE (rapid amplification of cloned DNA ends) to obtain the 5' end of Nvβ-catenin (SMART RACE cDNA amplification kit, Clontech). This fragment was digested with *Kpn*I and *Hind*III and used in a three-way ligation with the *Hind*III/*Not*I-digested 3' fragment and *Kpn*I/*Not*I-digested pBSKII (Stratagene). This plasmid was used as template for Vent DNA polymerase (NEB)-mediated polymerase chain reaction (PCR) using forward primer 5'-CGGGATCCATGGAGACACACGGTATG-3' and reverse primer

5'-CGGGATCCGTTTCGGGAATGTAGTAGG-3' to obtain a Nvβ-catenin fragment that contained the translation start site and all the armadillo repeats, but was missing the 3' transactivation domain. The PCR product was digested with *Bam*HI, and ligated into *Bam*HI-digested pCS2+ vector containing the coding sequence for GFP at the *Clal*/*Eco*RI sites to produce pCS2Nvβ-cat-GFP. Fidelity of all PCR reactions was verified by sequencing. The activated *Xenopus* β-catenin-GFP construct was made by digesting XBC69 (ref. 22) (a gift from D. Kimelman) with *Clal* and *Eco*RI to release the six Myc tags, and replacing it with GFP. The *Lytechinus variagatus* cadherin<sup>5</sup>, *Xenopus* β-catenin-engrailed<sup>25</sup> and *Xenopus* β-catenin-GFP<sup>20</sup> constructs have been previously described. All constructs were linearized before mRNA synthesis.

**Gamete handling**

Fertilized eggs were dejellied with 2% cysteine in one-third strength sea water for 10 min, and rinsed three times in one-third strength sea water in preparation for microinjection or immunohistochemistry.

**mRNA synthesis, microinjection and fluorescence microscopy**

Linearized constructs were used as templates for SP6-dependent RNA transcription using the mMessage mMachine mRNA synthesis kit from Ambion according to the vendor's specifications. Synthetic mRNA was prepared for microinjection as previously described<sup>28</sup>. mRNA was injected at a final concentration of 1.0 μg μl<sup>-1</sup> with 0.2 μg μl<sup>-1</sup> rhodamine dextran in 40% glycerol under a Zeiss SV-11 fluorescent dissecting microscope. Embryos were raised in one-third strength sea water until the desired stage, at which they were examined under a Zeiss Axioplan compound microscope or a Zeiss 510 laser scanning confocal microscope. Digital images were obtained with either a Zeiss Axiocam or a Nikon Coolpix 990 digital camera.

**Immunocytochemistry**

Embryos at different stages of development were fixed in paraformaldehyde (MEMPf) and post-fixed with Dent's fixative as described for *Xenopus* embryos<sup>29</sup>. Briefly, the embryos were initially fixed in MEMPf for 1 h followed by Dent's fixative for 15 min. The embryos were bleached for 30 min in two parts Dent's fixative and one part 30% hydrogen peroxide. Fixed and rinsed embryos were blocked in 5% normal donkey serum/0.05% Tween-20 in phosphate buffered saline (PBS) at pH 7.4. Embryos were incubated in affinity purified anti-*Xenopus* β-catenin antibody<sup>30</sup> at 4 °C overnight. Embryos were then rinsed three times in blocking buffer and incubated in horseradish peroxidase-conjugated anti-rabbit donkey secondary antibody (Jackson ImmunoResearch). After 1 h of incubation in the secondary antibody, embryos were rinsed and the staining was developed using DAB substrate. To verify that the primary antibody was recognizing Nvβ-catenin, it was pre-adsorbed with a bacterially produced Nvβ-catenin fusion protein before incubation with embryos. Rinsed embryos were mounted in methyl salicylate and observed using a Zeiss Axiovert 200 microscope using differential interference contrast optics. Stained embryos were photographed using a Nikon Coolpix 995 digital camera.

Received 25 June; accepted 6 October 2003; doi:10.1038/nature02113.

- Miller, J. R. & Moon, R. T. Signal transduction through beta-catenin and specification of cell fate during embryogenesis. *Genes Dev.* **10**, 2527–2539 (1996).
- Huelsken, J. & Birchmeier, W. New aspects of Wnt signalling pathways in higher vertebrates. *Curr. Opin. Genet. Dev.* **11**, 547–553 (2001).
- Polakis, P. Wnt signalling and cancer. *Genes Dev.* **14**, 1837–1851 (2000).
- Wikramanayake, A. H., Huang, L. & Klein, W. H. beta-catenin is essential for patterning the maternally specified animal-vegetal axis in the sea urchin embryo. *Proc. Natl Acad. Sci. USA* **95**, 9343–9348 (1998).
- Logan, C. Y., Miller, J. R., Ferkowicz, M. J. & McClay, D. R. Nuclear beta-catenin is required to specify vegetal cell fates in the sea urchin embryo. *Development* **126**, 345–357 (1999).
- Imai, K., Takada, N., Satoh, N. & Satou, Y. Beta-catenin mediates the specification of endoderm cells in ascidian embryos. *Development* **127**, 3009–3020 (2000).
- Thorpe, C. H., Schlesinger, A., Carter, J. C. & Bowerman, B. Wnt signalling polarizes an early *C. elegans* blastomere to distinguish endoderm from mesoderm. *Cell* **90**, 695–705 (1997).
- Rocheleau, C. E. *et al.* Wnt signalling and an APC related gene specify endoderm in early *C. elegans* embryos. *Cell* **90**, 707–716 (1997).
- Schneider, S., Steinbeisser, H., Warga, R. M. & Hausen, P. Beta-catenin translocation into nuclei demarcates the dorsalizing centres in frog and fish embryos. *Mech. Dev.* **57**, 191–198 (1996).
- Miyawaki, K. *et al.* Nuclear localization of beta-catenin in vegetal pole cells during early embryogenesis of the starfish *Asterina pectinifera*. *Dev. Growth Differ.* **45**, 121–128 (2003).
- Medina, M., Collins, A. G., Silberman, J. D. & Sogin, M. L. Evaluating hypotheses of basal animal phylogeny using complete sequences of large and small subunit rRNA. *Proc. Natl Acad. Sci. USA* **98**, 9707–9712 (2001).
- Collins, A. G. Evaluating multiple alternative hypothesis for the origin of Bilateria: An analysis of 18S rRNA molecular evidence. *Proc. Natl Acad. Sci. USA* **95**, 15458–15463 (1998).
- Hand, C. & Uhlinger, K. R. The culture, sexual and asexual reproduction, and growth of the sea anemone *Nematostella vectensis*. *Biol. Bull.* **182**, 169–176 (1992).
- Goldstein, B. & Freeman, G. Axis specification in animal development. *Bioessays* **19**, 105–116 (1997).
- Knoll, A. & Carroll, S. Early animal evolution: emerging views from comparative biology and geology. *Science* **284**, 2129–2137 (1999).
- Hobmayer, B. *et al.* WNT signalling molecules act in axis formation in the diploblastic metazoan *Hydra*. *Nature* **407**, 186–189 (2000).
- Klein, P. S. & Melton, D. A. A molecular mechanism for the effect of lithium on development. *Proc. Natl Acad. Sci. USA* **93**, 8455–8459 (1996).
- Kao, K. R. & Elinson, R. P. The legacy of lithium effects on development. *Biol. Cell* **90**, 585–590 (1998).
- Schneider, S. Q., Finnerty, J. R. & Martindale, M. Q. Protein evolution: structure-function relationships of the oncogene beta-catenin in the evolution of multicellular animals. *J. Exp. Zool. B* **295**, 25–44 (2003).

20. Miller, J. R. & Moon, R. T. Analysis of the signalling activities of localization mutants of beta-catenin during axis specification in *Xenopus*. *J. Cell Biol.* **139**, 229–243 (1997).
21. Weitzel, H. E. & Etensohn, C. A. beta-catenin is differentially degraded along the animal-vegetal axis of early sea urchin embryos in a GSK-3b-dependent manner. *Dev. Biol.* **247**, 479a (2002).
22. Yost, C. *et al.* The axis-inducing activity, stability, and subcellular distribution of beta-catenin is regulated in *Xenopus* embryos by glycogen synthase kinase 3. *Genes Dev.* **10**, 1443–1454 (1996).
23. Dings, Y. & Dale, T. Wnt signal transduction: kinase cogs in a nano-machine? *Trends Biochem. Sci.* **27**, 327–329 (2002).
24. Heasman, J. *et al.* Overexpression of cadherins and underexpression of beta-catenin inhibit dorsal mesoderm induction in early *Xenopus* embryos. *Cell* **79**, 791–803 (1994).
25. Montross, W. T., Ji, H. & McCrea, P. D. A beta-catenin/engrailed chimera selectively suppresses Wnt signalling. *J. Cell Sci.* **113**, 1759–1770 (2000).
26. Freeman, G. & Miller, R. L. Hydrozoan eggs can only be fertilized at the site of polar body formation. *Dev. Biol.* **94**, 142–152 (1982).
27. Larabell, C. A. *et al.* Establishment of the dorso-ventral axis in *Xenopus* embryos is presaged by early asymmetries in beta-catenin that are modulated by the Wnt signalling pathway. *J. Cell Biol.* **136**, 1123–1136 (1997).
28. Mao, C.-A. *et al.* Altering cell fates in sea urchin embryos by overexpressing SpOx, an orthodenticle-related protein. *Development* **122**, 1489–1498 (1996).
29. Klymkowsky, M. W. & Hanken, J. Whole-mount staining of *Xenopus* and other vertebrates. *Methods Cell Biol.* **36**, 419–441 (1991).
30. McCrea, P. D., Briher, W. M. & Gumbiner, B. M. Induction of a secondary body axis in *Xenopus* by antibodies to beta-catenin. *J. Cell Biol.* **123**, 477–484 (1993).

**Supplementary Information** accompanies the paper on [www.nature.com/nature](http://www.nature.com/nature).

**Acknowledgements** We thank Y. Marikawa, B. Klein and members of our laboratories for critical reading of the manuscript and for suggestions and P. McCrea for the gift of affinity-purified  $\beta$ -catenin antibody. This work was supported by grants from the NSF and the Hawaii Community Foundation to A.H.W. and by grants from the NSF and NASA to M.Q.M.

**Competing interests statement** The authors declare that they have no competing financial interests.

**Correspondence** and requests for materials should be addressed to A.H.W. ([athula@hawaii.edu](mailto:athula@hawaii.edu)) or M.Q.M. ([mqmartin@hawaii.edu](mailto:mqmartin@hawaii.edu)).

## Angiotensin-converting enzyme 2 is a functional receptor for the SARS coronavirus

Wenhui Li<sup>1</sup>, Michael J. Moore<sup>1</sup>, Natalya Vasilieva<sup>2</sup>, Jianhua Sui<sup>3</sup>, Swee Kee Wong<sup>1</sup>, Michael A. Berne<sup>4</sup>, Mohan Somasundaran<sup>5</sup>, John L. Sullivan<sup>5</sup>, Katherine Luzuriaga<sup>5</sup>, Thomas C. Greenough<sup>5</sup>, Hyeryun Choe<sup>2</sup> & Michael Farzan<sup>1</sup>

<sup>1</sup>Partners AIDS Research Center, Brigham and Women's Hospital, Department of Medicine (Microbiology and Molecular Genetics), <sup>2</sup>Perlmutter Laboratory, Pulmonary Division, Children's Hospital, Department of Pediatrics,

<sup>3</sup>Dana-Farber Cancer Institute, Department of Medicine, Harvard Medical School, Boston, Massachusetts 02115, USA

<sup>4</sup>Tufts University Core Facility, Tufts University School of Medicine, Boston, Massachusetts 02111, USA

<sup>5</sup>Program in Molecular Medicine, University of Massachusetts Medical School, Worcester, Massachusetts 01605, USA

Spike (S) proteins of coronaviruses, including the coronavirus that causes severe acute respiratory syndrome (SARS), associate with cellular receptors to mediate infection of their target cells<sup>1,2</sup>. Here we identify a metallopeptidase, angiotensin-converting enzyme 2 (ACE2)<sup>3,4</sup>, isolated from SARS coronavirus (SARS-CoV)-permissive Vero E6 cells, that efficiently binds the S1 domain of the SARS-CoV S protein. We found that a soluble form of ACE2, but not of the related enzyme ACE1, blocked association of the S1 domain with Vero E6 cells. 293T cells transfected with ACE2, but not those transfected with human immunodeficiency virus-1 receptors, formed multinucleated syncytia with cells expressing S protein. Furthermore, SARS-CoV replicated efficiently on ACE2-transfected but not

mock-transfected 293T cells. Finally, anti-ACE2 but not anti-ACE1 antibody blocked viral replication on Vero E6 cells. Together our data indicate that ACE2 is a functional receptor for SARS-CoV.

So far two types of coronavirus surface receptor have been identified<sup>5</sup>. The group II coronavirus mouse hepatitis virus (MHV) uses murine carcinoembryonic antigen-related cell adhesion molecules (CEACAMs), members of the immunoglobulin superfamily of receptors<sup>6</sup>. A number of group I coronaviruses, for example human coronavirus 229E, transmissible gastroenteritis virus and feline infectious peritonitis virus, require the zinc metalloprotease aminopeptidase N (APN, CD13) for entry into their target cells<sup>7–9</sup>. Recently, a distinct coronavirus has been identified as the aetiological agent of SARS, an acute pulmonary syndrome characterized by an atypical pneumonia that results in progressive respiratory failure and death in close to 10% of cases<sup>10–13</sup>. Analysis of the SARS-CoV genome suggests that this virus does not belong to any of the three defined coronavirus groups, and that the SARS-CoV S protein is similarly distinct<sup>14,15</sup>. Similar to the analogous human immunodeficiency virus (HIV) and influenza proteins, the S proteins of some coronaviruses—including MHV and the group III coronavirus infectious bronchitis virus—are cleaved into two subunits (S1 and S2) by a cellular protease in virus-producing cells<sup>16,17</sup>. The S proteins of other coronaviruses, including those of group I and probably SARS-CoV, are not cleaved in virus-producing cells<sup>14,15,18</sup>. Nonetheless, S1 and S2 domains of these latter S proteins can be identified through their homology with the S1 and S2 subunits of cleaved coronavirus S proteins. The S1 domains of all characterized coronaviruses mediate an initial high-affinity association with their respective receptors<sup>19–21</sup>.

The African green monkey kidney cell line Vero E6 permits replication of SARS-CoV<sup>10</sup>. We first investigated whether the S1 domain of the SARS-CoV S protein could bind to Vero E6 cells. Figure 1a demonstrates that a protein expressing residues 12–672 of the SARS-CoV S protein, fused to the Fc domain of human immunoglobulin- $\gamma$ 1 (IgG1; S1-Ig), specifically recognized a moiety present on Vero E6 cells but did not bind human kidney 293T cells. Using this same fusion protein (Fig. 1c) or a carboxy terminally tagged form of the S1 domain (Fig. 1b), a protein band of approximately 110 kDa could be immunoprecipitated from metabolically labelled Vero E6 cells lysed with 0.3% *n*-decyl- $\beta$ -D-maltopyranoside in phosphate-buffered saline. When the immunoprecipitated protein was incubated with PNGase F, an enzyme that removes *N*-glycosylation, two bands were observed at approximately 80–85 and 100 kDa (Fig. 1c, lanes 3 and 4).

We then analysed the 110 kDa band by trypsin digestion and mass spectrometry. Three human proteins were identified whose sequences were consistent with the masses of tryptic fragments obtained from this band. Two of these proteins, myosin 1b and major vault protein, do not localize to the cell surface and are ubiquitously expressed, therefore we did not analyse them further. Eight independent tryptic fragments consistent with sequences comprising 17% of the amino acid sequence of human ACE2 were also identified (Supplementary Information). Because both the tissue distribution and subcellular localization of ACE2 are appropriate for a receptor for SARS-CoV<sup>3,22,23</sup>, we cloned it from complementary DNA obtained from human lung for further analysis.

293T cells transfected with plasmid expressing ACE2, but not those transfected with vector alone, were specifically recognized by S1-Ig (Fig. 2a). A soluble form of ACE2, but not that of the related enzyme ACE1, blocked the association of S1-Ig with Vero E6 cells (Fig. 2b). Furthermore, S1-Ig immunoprecipitated a soluble form of ACE2 (Fig. 2c, lane 5) that was recognized by an anti-ACE2 antibody (lane 8). When the approximately 110 kDa soluble form of ACE2 was incubated with PNGase F, an 85 kDa band was observed (Fig. 2c, lanes 5 and 6), indicating that the lower band observed in